Turbularization of an Acoustic Boundary Layer on a Transpiring Surface

Robert A. Beddini* and Ted A. Roberts†
University of Illinois at Urbana-Champaign, Urbana, Illinois

Turbularization of an acoustic boundary layer (Stokes layer) on impermeable and permeable surfaces is analytically considered. The theoretical approach utilizes a second-order closure model of turbulence. Both an approximate, closed-form solution and a more comprehensive finite-difference solution of the time-dependent, parabolic, one-dimensional governing equations are obtained. For simple acoustic boundary layers on impermeable surfaces, both the approximate solution and the numerical results for the critical acoustic Mach number required for turbulent transition are qualitatively confirmed by experiment. The calculations for acoustic boundary layers with transpiration (injection) indicate a substantial reduction of the acoustic Mach number required for transition, up to a limiting injection velocity that is frequency dependent. The results may provide a mechanism for flow-related combustion instability in practical systems, particularly solid propellant rockets, since turbularization of the near-surface combustion zone could result at relatively low-acoustic Mach numbers.

Nomenclature

a = sonic speed
c_p = specific heat at constant pressure
f = frequency, Hz
h = specific sensible enthalpy
k = thermal conductivity
k_s = equivalent sand roughness height
p = static pressure
q = turbulence intensity, $(\overline{u'^i u'_i})^{1/2}$
q_m = maximum value of q
R = inner radius of a cylindrical duct
Re_c = axial-flow Reynolds number, $\bar{\rho}_c \bar{u}_c \delta/\bar{\mu}_c$
Re_s = injection Reynolds number, $\bar{\rho}_s \bar{v}_s \delta/\bar{\mu}_s$
Re_t = turbulence Reynolds number, $\bar{\rho} q \Lambda/\mu$
R_u = universal gas constant
t = time
T = static temperature
u_j = velocity vector (u,v,w)
x_j = coordinate vector (x,r,z)
x_o = axial distance at which computational initial conditions are specified
y = distance from surface
ϕ = characteristic length scale
Λ = turbulence macrolength scale
μ = viscosity
ν = kinematic viscosity
ρ = density
σ = k/c_p
σ_v = $[\overline{v'v'}/\bar{v}^2|_s]^{1/2}$
τ = turbulence shear stress
$< >$ = time mean of variable

Superscripts
$-$ = average of variable over turbulent fluctuations
$'$ = turbulent fluctuating value of variable
$''$ = acoustic fluctuating value of variable

Subscripts
a = acoustic
c = duct centerline
e = value at edge ob boundary layer
h = condition at port head end
m = maximum absolute value
s = condition at surface
, = differentiation

I. Introduction

OSCILLATORY flows in ducts can be sustained by a variety of interactions. These range from purely fluid-dynamically induced motions (e.g., large-scale vortex shedding or shockwave instability), to the more energetic motions possible with diabatic flows. Particularly severe oscillations can occur in solid propellant rocket chambers, for example, wherein the oscillatory motion can be driven by interactions with the substantial energy release inherent in near-surface combustion processes.

Prior analytical work in "combustion" instability in solid rockets has identified some of the mechanisms that can produce velocity-field coupling to the overall instability process (see, for example, the review by Culick[1]). These studies have shown that for a simple longitudinal standing acoustic wave in a duct, a Rayleigh diabatic instability criterion can result, which is dependent on the oscillatory motion of the gas column. Since the energy release occurs in the near-surface region, analytical work has addressed acoustic boundary-layer effects on propellant combustion response (see, for example, Lengellé[2]). Implicit in several response function analyses is the assumption that the acoustic boundary layers behave quasisteadily and in phase with the longitudinal acoustic velocity outside the boundary layer.

Recent work on combustion-flowfield interactions in solid rocket chambers has analytically and experimentally examined fundamental fluid-dynamic aspects of mean flow, acoustic wave and turbulence behavior. Hydrodynamically modeling the flow with a semienclosed, porous-walled duct (with large injection through the wall) Brown et al.[3,4] experimentally confirmed the transitional behavior of the mean flow predicted in Ref. 5. The major emphasis of this nonreactive flow experiment was to investigate the effect of low- and moderate-amplitude forced acoustic oscillations on the flow, using both hot-wire anemometry and surface-mounted hot-film sensors.

Basing their conclusions on the surface sensor measure-

Received Nov. 13, 1986; revision received Aug. 5, 1987.

*Professor, jointly appointed to the Departments of Mechanical and Industrial Engineering. Member AIAA.
†Graduate Research Assistant, Department of Aeronautical and Astronautical Engineering. Student Member AIAA.

ments, Brown and co-workers suggested that near surface turbulence produced by the mean-flow transition process appeared to "destroy" the coherent response of the sensors downstream of transition. Consequently, for low acoustic amplitudes, a surface response capable of inducing instability would most probably originate in the head end (pretransition) section of a rocket chamber. However, it is noted that for large axial distances, low-amplitude acoustic signals appear to be resurrected in the post-transition region. Lower amplitude harmonics of the driving frequency were observed by Brown and co-workers in both the surface and hot-wire measurements. Their existence is consistent with the nonlinear behavior of a (potentially thick) acoustic boundary layer (Stokes layer).

Analyses of laminar acoustic boundary-layer phenomena involved in propellant response have been offered by Flandro,[6] Glick and Renie,[7] Ben Reuven,[8] and Hedge et al.[9] Baum and Levine[10] utilized a full unsteady Navier-Stokes solution method; their results showed a Stokes layer persisting even in the presence of strong injection velocities. The thickness of the Stokes layer was of the same order as the Stokes layer for noninjected flow. The presence of vortices above the acoustic boundary layer were also indicated in the results. Although several aspects of these analyses are interesting, the following important point is noted. Simple scaling estimates of the laminar acoustic boundary layer height (the Stokesian thickness) $\delta_a = \sqrt{(\nu/f)}$ indicates that δ_a is well above the gas-phase flame height except for very high frequencies ($f \geq 10^4$ Hz). Consequently, minimal acoustic velocity interaction with combustion would be expected at low to intermediate frequencies as indicated, for example, by the more detailed analysis of Ref. 6. Although this does not preclude "velocity coupled" instability resulting from laminar interactions (whether linear or nonlinear), it does suggest that other mechanisms of interaction should be explored.

Consequently, the potential for the laminar acoustic boundary-layer to undergo transition to turbulence is considered. It is well established that, for piston-driven, closed-duct flows (in which there is negligible mean axial flow), longitudinal acoustic waves of a few percent relative pressure amplitude can induce turbulence within the Stokes layer. The literature review and independent data of Merkli and Thomann[11], for example, confirm a critical amplitude which varies as $\sqrt{f}$ for this type of simple acoustic motion. Thus, for fixed amplitude, lower frequency disturbances are more likely to produce turbulence.

It is known from studies of quasisteady propellant/flowfield interactions that even small levels of turbulence within the combustion zone can appreciably enhance propellant combustion rates. Whether acoustically induced turbularization can occur in actual rocket chambers depends on several complex effects including the presence of large injection rates, surface roughness and, of course, the specific type of combustion process. In one experiment,[12] values of the threshold velocity for propellant response ("acoustic erosivity") were lowered by a factor of two relative to steady-state conditions.

The objective of the present analysis is to consider, under several simplifying assumptions, the general trends of acoustic boundary-layer turbularization on a permeable surface in the presence of large injection rates. Though pertinent to the issues discussed previously, the posed problem is more fundamental and of potentially broader interest.

II. Analysis

The motion of a perfect gas described by the Navier-Stokes equations is considered. An arbitrary dependent variable $g(x_i,t)$ is decomposed according to the notation

$$g(x_i,t) = \bar{g}(x_i, t) + g'(x_i, t)$$

with

$$\bar{g} = <g(x_i, t)> + g''(x_i, t)$$

In these equations, g' is the turbulent fluctuation, $\bar{g}$ the ensemble average, g'' the acoustic (deterministic) component, and $<g>$ the long-time mean. The remainder of this section is divided into two parts. The first considers order-of-magnitude analysis of the problem and derivation of an approximate relation for critical amplitude of transition from the turbulence model equations. The second part discusses the equations and method used for a more comprehensive numerical solution of the acoustic boundary layer in the presence of transpiration.

A. Order of Magnitude Analysis[19]

Neglecting third-order correlations and the axial derivatives of molecular and turbulent stresses, the $<>$ average of the axial momentum equation is

$$\frac{\partial}{\partial x}(<\rho><u><u> + <\rho><u''u''> + <u><\rho''u''> + <u><\rho''u''>)$$
$$+\frac{\partial}{\partial y}(<\rho><u><v> + <\rho><u''v''> + <u><\rho''u''> + <v><\rho''u''>)$$
$$= -\frac{\partial <p>}{\partial x} + \frac{\partial}{\partial y}\left(<\mu>\frac{\partial <u>}{\partial y}\right) + \frac{\partial <\tau>}{\partial y} \qquad (1)$$

where the mean turbulent shear stress is $<\tau> = -<\rho><u'v'>$ (neglecting turbulent density correlations). The equation for the acoustic component (u'') is, to first order:

$$\underset{(1)}{<\rho>\frac{\partial u''}{\partial t}} + \underset{(2)}{(<\rho>u'' + <u>\rho'')\frac{\partial <u>}{\partial x}} + \underset{(3)}{u''\frac{\partial}{\partial x}(<\rho><u>)}$$
$$+ \underset{(4)}{<\rho><u>\frac{\partial u''}{\partial x}} + \underset{(5)}{(<\rho>v'' + <v>\rho'')\frac{\partial <u>}{\partial y}}$$
$$+ \underset{(6)}{u''\frac{\partial}{\partial y}(<\rho><v>)} + \underset{(7)}{<\rho><v>\frac{\partial u''}{\partial y}} = \underset{(8)}{\frac{-\partial p''}{\partial x}}$$
$$+ \underset{(9)}{\frac{\partial}{\partial y}\left(<\mu>\frac{\partial u''}{\partial y}\right)} + \underset{(10)}{\frac{\partial \tau''}{\partial y}} \qquad (2)$$

where $\tau'' \simeq -<\rho>\overline{u'v'}$.

In Eq. (1), the second-order correlations arising from the unsteady motion can produce virtual stresses and convective fluxes analogous to those produced by the turbulent motion alone. These correlations induce the classical phenomenon of "acoustic streaming,"[14-15] wherein a component of the mean flow is driven by acoustic motion. Of potentially more importance to propellant combustion are the analogous second-order terms which appear in the equation for the transport of thermal energy in the propellant flame zone. While these thermal transport effects will not be analyzed in this study, examples of their importance to effective steady-state heat transfer may be found in the literature (see, for example, Ref. 13). The effects of steady-state enhancements to heat transfer from acoustic streaming effects have not been considered with respect to the reactive environment in rocket engines, although it is possible that these effects could also produce a coupling mechanism for instability.

The remainder of this analysis will be concerned with Eq. (2) and the relative importance of various terms within the acoustic boundary layer. To simplify this equation further, it will be assumed that the density in the region of interest is approximately constant, and that the v'' produced by propel-

lant response is negligible. These assumptions would necessarily be removed in considering a comprehensive propellant velocity response analysis.

The magnitudes of the terms in Eq. (2) are estimated by normalizing the velocities to a_o, the chamber length to L, chamber radius to δ, and utilizing the continuity equation and the assumption of a standing first longitudinal acoustic mode. It is also assumed that the turbulence shear stress may be scaled by $\tau'' = c_\tau <\rho> u''^2$, where $|c_\tau| \ll 1$. The respective orders of the terms in Eq. (2) are then

$$\{1,\ <M>,\ <M>,\ <M>,\ (\delta_a/\delta)<M>,\ <M>,$$

$$(a_0/f\delta_a)<M_s>,\ 1,\ \nu/f\delta_a^2,\ c_\tau a_0/(f\delta_{a,\,\mathrm{turb}})\ M''\}$$

The order unity terms (1) and (8) recover the inviscid acoustic mode solution in the central region of the duct. A considerable simplification results if $<M>$ is small, since terms (2)–(6) may be dropped without fundamentally altering boundary-layer characteristics retained in terms (7), (9), and (10). (It is important to note that the maximum response to the surface sensors in Ref. 4 occurs in the head-end region, where $<M>$ is $\lesssim 0.1$.) Neglecting for the moment the transverse convection and turbulence terms, it is seen that for the viscous term to be of order unity implies the Stokes estimate

$$\delta_a \sim \left(\frac{\nu}{f}\right)^{1/2} \tag{3}$$

and is the smallest possible laminar boundary-layer height of the problem. The effects of injection on the acoustic boundary layer [provided largely by term (7)] can be substantial and even dominate. The ratio between the convection and viscous terms in Eq. (3) is of the order 10 under conditions of interest.

The additional shear stress provided by term (10) in Eq. (2), as well as the analogous additional heat flux appearing in the energy equation, result from possible turbulent motions. Further, it is noted that term (10) is the only term which depends on the amplitude of the acoustic motion. (The acoustic amplitude M'' is a linear scaling parameter of all other terms but occurs quadratically in the turbulent shear term.) This dependence helps to pose the question of a possible relation to nonlinear stability phenomena.

As noted in Ref. 11, there are a few approaches that can be employed to obtain a stability or transition criterion for the acoustic boundary layer. In the approach adopted here, the second-order modeling equations employed in Ref. 3 are considered (see also Sec. IIB). Preliminary operations and assumptions are summarized as follows. Equations for the velocity correlations $\overline{u_i' u_j'}$ are contracted to obtain an equation for the turbulence intensity $q^2 = \overline{u_i' u_i'}$. Fluid material properties are assumed constant, and the turbulence (or preturbulent disturbance level) is assumed small so that third- and higher-order velocity correlations may be neglected. It is also assumed as an approximation that

$$\overline{u'u'} = a_{uu} q^2$$

$$\overline{v'v'} = a_{vv} q^2$$

$$\overline{u'v'} = a_{uv} q^2$$

where a_{uu}, a_{vv}, and a_{uv} are constants. Substituting these relations into the q^2 equation, taking the mean flow to be negligible, and applying boundary-layer assumptions for a quasiplanar condition yields:

$$\rho\left(\frac{\partial q^2}{\partial t} + u''\frac{\partial q^2}{\partial x} + v''\frac{\partial q^2}{\partial y}\right) + 2\rho\, q^2\left(a_{uu}\frac{\partial u''}{\partial y} + a_{uv}\frac{\partial u''}{\partial y}\right)$$

$$= -2A\frac{\mu q^2}{\Lambda^2} + \frac{\mu \partial^2 q}{\partial y^2} \tag{4}$$

where Λ is the disturbance macrolength scale and A a constant used in modeling low turbulent Reynolds number dissipation. The approximation $\Lambda = C_\Lambda \delta_a$ [where δ_a is specified by Eq. (3)] is also employed to evaluate the maximal effective length scale appropriate for the acoustic boundary layer.

Equation (4), which is linear in q^2, may be order-of-magnitude scaled in the same manner as Eq. (2). The requirement that $\rho \mathrm{D}q^2/\mathrm{D}t = 0$ (for neutral stability) may be imposed if the Reynolds number $u''\delta_a/\nu \lesssim 0(1)$. The order-of-magnitude analysis indicates that the fifth (production) term on the left-hand side and the first (dissipation) term on the right-hand side of Eq. (2) are dominant, resulting in the stability criterion

$$M''_{\mathrm{cr}} = \frac{A}{(-a_{uv})C_\Lambda^2}\frac{(f\nu)^{1/2}}{a_o} = K\frac{(f\nu)^{1/2}}{a_o} \tag{5}$$

Utilizing the turbulence modeling constants specified in the Appendix of Ref. 3 (i.e., $A = 3.25$, $C_\Lambda = 0.17$), and estimating $a_{uv} = -0.15$ from fully developed flate-plate turbulent boundary layer flows, yields an estimate of $K = 750$. Merkli and Thomann[11] cite prior experimental values of K ranging from 188 to 915 and obtained the value $K = 501$ in their own experiments. The constant K in Eq. (5) is related to the Merkli and Thomann constant A_c by $K = A_c\sqrt{(2\pi)/2}$. They speculated that the variation in K observed in prior studies could be caused by variations in the roughness of the duct surface and demonstrated that disturbances caused by the anemometer probe can also appreciably affect K.

The critical Mach number given by Eq. (5) is shown in Fig. 1 together with the data of Merkli and Thomann. The functional dependence is correct, and even the very approximate estimates of physical constants and empirical parameters yield quantitative agreement to within several percent of the data. To the authors' knowledge, the derivation of an approximate transition relation from linearizing this type of complex turbulence model is novel.

B. Computational Analysis

The second-order turbulence closure approach developed by Donaldson et al.[16] and Varma et al.[17] was implemented in Ref. 3 as a parabolized model for calculating statistically stationary, compressible transitional flows in porous walled ducts with large injection rates. The assumptions and order-of-magnitude analysis of the previous section again yield a parabolic equation system for the present acoustic boundary-layer problem. Computationally, the axial convection terms $\overline{\rho u}\,\partial g/\partial x$ (where g is an arbitrary dependent variable) are replaced by $\bar{\rho}\,\partial g/\partial t$ for the present case. With the exception of $\partial \bar{p}/\partial x$ in the momentum equation, all other axial derivatives are taken to be null. The continuity equation

$$\frac{\partial \bar{\rho}}{\partial t} + \frac{1}{r^\nu}\frac{\partial}{\partial r}\left[r^\nu(\overline{\rho v} + \overline{\rho' v'})\right] = 0$$

and the $\partial \bar{p}/\partial t$ term on the right-hand side of the energy equation is retained, however, for planned work involving energetic flows.

The parabolic differential equation system may be considered in the functional form

$$\bar{\rho}\frac{\partial g}{\partial t} + \bar{\rho}\,\bar{v}\frac{\partial g}{\partial r} = \frac{1}{r^\nu}\frac{\partial}{\partial r}\left(r^\nu \bar{\mu}_g \frac{\partial g}{\partial r}\right) + G_g(f) \tag{6}$$

where $g = \{\bar{u},\ \bar{h},\ \overline{u'u'},\ \overline{v'v'},\ \overline{w'w'},\ \overline{u'v'},\ \overline{h'u'},\ \overline{h'v'},\ \overline{h'h'}\}^T$, u, v, and w are the axial, radial, and circumferential velocity components, respectively, ν the index for planar or axisymmetric geometry, ρ the density, and $h = c_p T$ is the specific static enthalpy. The molecular transport coefficient μ represents the dynamic viscosity (μ) or the thermal conductivity parameter $\sigma = k/c_p$ as appropriate for each equation. Nevertheless, not all of the molecular diffusion terms for each

equation in the system may be cast in the form shown in Eq. (2). Those that do not conform are implicitly contained within the complex functions G_g, which also represent the sources, cross-coupling, and dissipation terms for the equations. Although the more general $(^{-})$ averaging is used in the above notation, the only mean velocity component retained is $\bar{v}$, which is nearly equal to $<v>$ in this study because of the approximately isothermal and isobaric conditions assumed.

The pressure along the duct, $\bar{p} = <p> + p''(x,t)$, is specified by the one-dimensional standing wave solution

$$p'' = \Pi_{ma} <p> \cos(n\pi x/L)\cos(2\pi ft) \qquad (7)$$

where Π_{ma} is the maximum relative acoustic pressure amplitude and $u_{ma} = \Pi_{ma} a_o/\gamma$. All calculations to be presented were performed at the velocity antinode of the first longitudinal mode. Material properties were those of air at standard conditions.

The turbulence length scale Λ, in this model, is algebraic and described[5] by a linear variation from its surface value, Λ_s ($\Lambda_s = 0$ for smooth walls), to a plateau level proportionate (with constant C_Λ) to the thickness of the shear flow. For the present analysis this thickness was defined as δ_{aa}, equal to the height above the surface where the boundary asymptotes to 99% of u_c''. For injected flows, however, waves are convected away from the surface. In these cases the first zero-crossing of u'' was taken as the effective δ_{aa}. The final values of δ_{aa} used in the length scale expression were smoothed by integrating in time. An alternative differential length-scale equation is desirable, but much has been written concerning problems with the low turbulent Reynolds number behavior of such equations.

Boundary conditions at the duct centerline (or centerplane) are the symmetry conditions, which for the posed systems are

$$\frac{\partial}{\partial r}[\bar{u},\ \bar{h},\ \overline{u'u'},\ \overline{v'v'},\ \overline{w'w'},\ \overline{h'h'},\ \overline{h'u'}] = 0$$

$$= \overline{u'v'} = \overline{h'v'}$$

Because of the final form of the governing equations, the requirement that $\bar{v} = 0$ be on the centerline (centerplane) is necessarily relaxed. At the duct surface, the static enthalpy corresponding to a given temperature is specified, and the mean injection velocity $\bar{v}_s$ is prescribed. The no-slip condition implies that all tangential velocity components and their correlations are zero. Experiments have confirmed that strong injection rates through a porous plate can produce pseudoturbulent disturbances which must be included in the ensemble average of the $\overline{v'v'}$ boundary condition. The parameter $\sigma_v^2 = \overline{v'v'}/\bar{v}^2$ was introduced in Ref. 3 to account for this important source of disturbance. All enthalpy correlations are null due to the prescribed uniform surface enthalpy.

The initial profile for the axial velocity component was taken to be the analytical solution (at $t = 0$) of Sexl and Uchida (in Schlichting[18]) for oscillatory flow in a cylindrical duct. Initial profiles of the normal Reynolds stresses were taken to be isotropic, and proportionate to the square of the initial velocity profile. The peak initial disturbance level, $q_{max}(t = 0,y)/u_{ma}$, was assumed to be 0.01 for all calculations reported here.

The implicit numerical procedure and adaptive grid are described in prior studies.[5] Except where noted, approximately 50 time steps per period were employed. The number of spatial nodes within the boundary layer varied from about 40 for laminar flows to about 75 for turbulent cases.

III. Results and Discussion

Normalized profiles of the axial velocity in the laminar acoustic boundary layer (f = 1000 Hz, δ_a = 180 μm) are shown for various times within a period in Fig. 2. The results display the classical phase shift and Richardson annular effects due to viscosity. The calculations were performed with 100 time steps per period and produce a relatively small computational error, principally outside the boundary layer and near the maxima in the acoustic velocity. Since a large number of calculations were needed for the transition studies, the number of time steps per period was halved for those calculations, and the error in the calculated acoustic velocity was then approximately doubled.

Figure 3 shows the profiles for a fully (cyclically) turbulent boundary layer at 100 Hz with $\Pi_{ma} = 0.125$. There is a noticeable diffusion of the Richardson effect and a pronounced increase in the velocity gradient near the surface. A protracted law-of -the-wall (logarithmic) region, however, is not observed.

Figure 4 shows normalized turbulence intensity profiles, q/u_{ma} in the boundary layer for the same conditions stated for Fig. 3. The calculated peaks in turbulence level are comparable to those calculated for steady-state flows ($\simeq$ 15%). Within computational accuracy, these peaks are symmetric with respect to $\pm\pi$ ft. A slight phase lag, on the order of 5–10 deg, exists between the intensity maxima and the rectified acoustic velocity $|u_c''|$. This lag increases at higher frequencies. Also note that the intensity decreases substantially, but is not predicted to vanish at the zero-crossings of u_c''.

Figure 5 shows turbulent velocity profiles for a Stokes layer with injection at f = 100 Hz, Π = 0.080, $<v>$ = 1 m/s. A pronounced Richardson effect is evident, surpassing even the laminar noninjected results. The estimated value of the effective boundary-layer thickness for this case is 5.5 mm

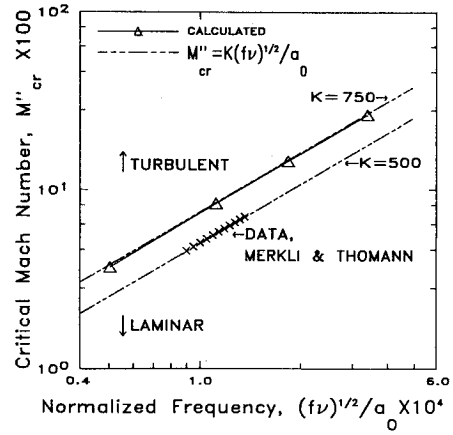

Fig. 1 Transition to turbulence for simple acoustic motion.

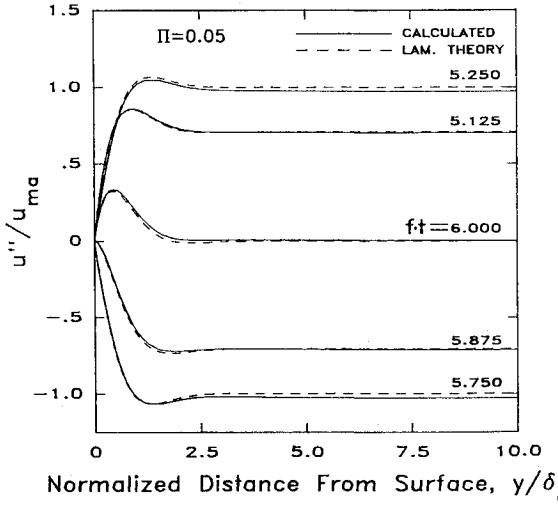

Fig. 2 Laminar velocity profiles in the acoustic boundary layer without injection.

(approximately $y/\delta_a = 14$ in the figure). The convective wave-train behavior shown is also evident in the laminar-injected Stokes layer calculations of Ref. 7.

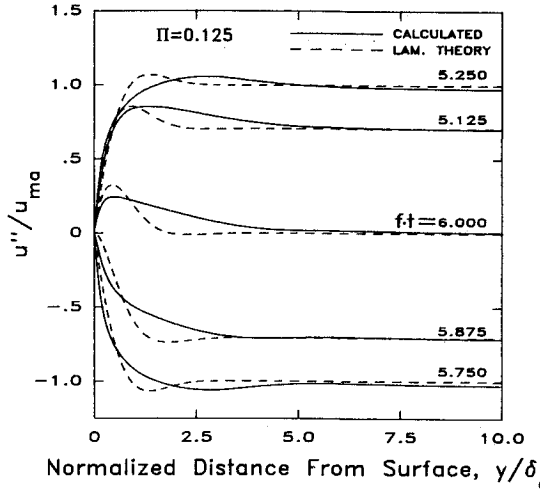

Fig. 3 Turbulent velocity profiles in the acoustic boundary layer without injection.

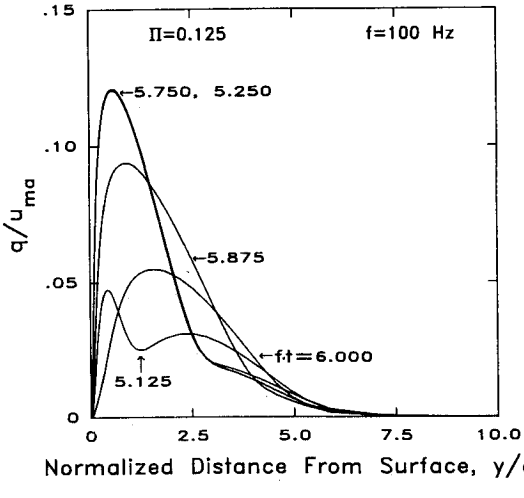

Fig. 4 Turbulence intensity profiles in the acoustic boundary layer without injection.

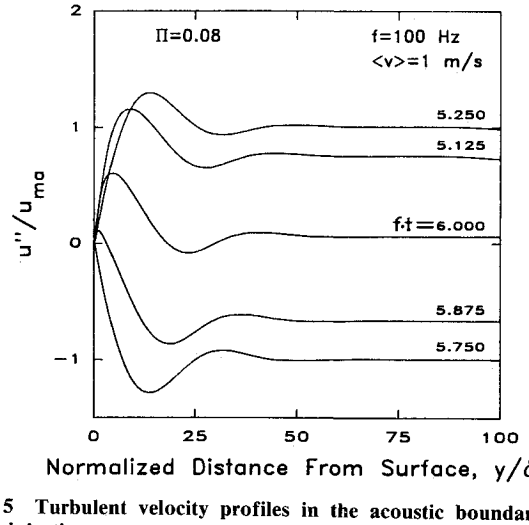

Fig. 5 Turbulent velocity profiles in the acoustic boundary layer with injection.

Figure 6 shows the corresponding normalized turbulence intensity profiles. Due, in part, to the enhanced Richardson effect, very large intensity levels ($\simeq 30\%$) are predicted. As turbulence is produced in the inner layer at a later time in the cycle, the velocity wave formed from an earlier cycle produces a harmonic wave in the intensity profile (ft = 5.125). A long tail is predicted due to large decay times and the fact that turbulence is beginning to accumulate at the computational centerline ($\delta = 5$ cm) where the symmetry condition is employed. In an actual duct-flow environment, the mean axial flow would convect these tails downstream as they interact with mean flow induced turbulence.

Calculated results for the critical acoustic Mach number at transition, $M''_{cr} = \Pi_{cr}/\gamma$, are shown in Fig. 1 together with the approximate relation and data for noninjected Stokes layers. The functional dependence is similar, but the proximity of the calculations to the $K = 750$ line is coincidental. Note, for example, that although not shown here, the numerical results display a dependence on the initial amplitude of turbulence assumed. "Transition" in the calculated results was determined by monitoring the growth or decay of initial turbulence from the initial value over several cycles. For the cases with injection, the growth rates were not as strongly dependent on Π as were those for the noninjected cases.

Critical Mach numbers for transition as a function of the normalized mean injection velocity, $< v > /\sqrt{f\nu}$, are shown in Fig. 7 for three frequencies, $f = 100$, 300, and 1000 Hz. A pronounced *decrease* in M''_{cr} is predicted with increasing injection

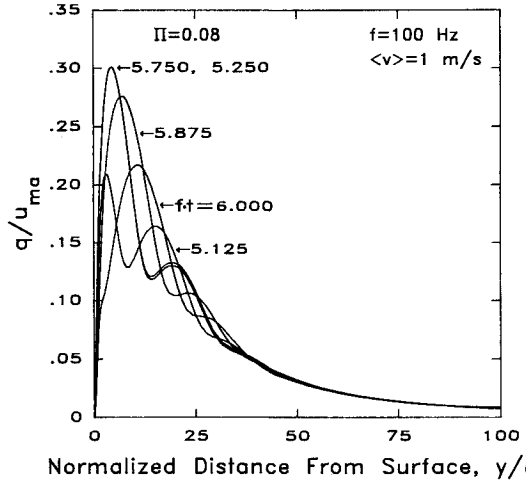

Fig. 6 Turbulence intensity profiles in the acoustic boundary layer with injection.

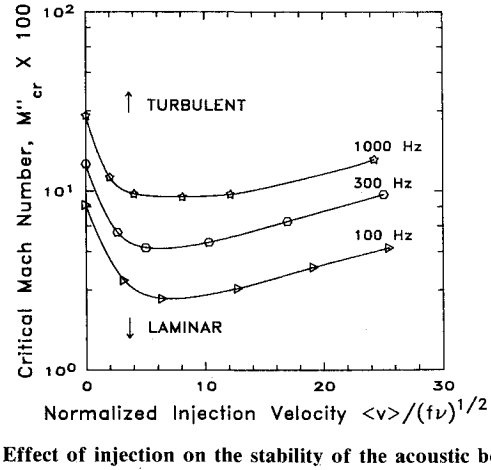

Fig. 7 Effect of injection on the stability of the acoustic boundary layer.

velocity, so that all curves exhibit a minimum that is frequency dependent. The minima are almost a factor of 3 below the M''_{cr} for noninjected Stokes layers. As an example, the 100 Hz noninjected Stokes layer is calculated to have $M''_{cr} = 0.083$. The minimum value of $M''_{cr} = 0.025$ occurs at $<v> \simeq 0.25$ m/s, while $M''_{cr} = 0.048$ at $<v> = 1.0$ m/s (the termination of the line at this frequency).

Even more informative are the same results for transition normalized not as a critical acoustic Mach number, but as a *critical acoustic Reynolds number*, $u_{ma}/\sqrt{fv}$. In this case, all three curves for frequency in Fig. 7 collapse onto a single line (to within computational precision), shown as the upper line in Fig. 8. This figure also shows results for finite levels of the surface disturbance parameter $\sigma_v = 0.035$ and 0.07 for two different transition criteria to be discussed. The accompanying value of Λ_s assumed in the calculations was 3×10^{-4} m. These values are viewed as realistic and perhaps conservative. It is not surprising that this finite disturbance effect, which continuously "feeds" the injected layer, is predicted to yield further reduction in critical acoustic Reynolds number, analogously to quasisteady flows.[3] As a specific example, the minimum critical Mach number for the 100 Hz case at $<v> = 0.20$ m/s is decreased to approximately 1% for $\sigma_v = 0.035$.

As mentioned earlier, it was more difficult to determine the value of M''_{cr} for cases with injection and finite levels of σ_v present. The first criterion employed consisted of monitoring the maximum turbulence level q_{max}/u_{ma} occurring at any height within the boundary layer. If this level attained a value of 0.07 or greater within three cycles, the flow was considered turbulent. Using this criterion, the $\sigma_v = 0$ lines were computed along with the alternating-dashed lines for $\sigma_v = 0.035$ and 0.07. While this criterion was satisfactory for the $\sigma_v = 0$ cases, it proved to be unsatisfactory for cases with finite levels of σ_v.

To illustrate this effect, Fig. 9 shows the variation of turbulence intensity vs normalized time at $y = \delta_a$, for three values of Π, $<v> = 0.25$ m/s and $\sigma_v = 0$. It is evident from the curves in Figs. 9a and 9b that a very small increase in π is able to cause the flow to transition to a cyclically turbulent condition.

When finite levels of σ_v are included, the determination of π_{cr} becomes more complicated. Figures 10a–10c are results for $<v> = 0.25$ m/s and $\sigma_v = 0.035$. Figure 10a is a case for which the turbulence bursts to a q/u_{ma} level of approximately 0.24 but then dissipates over 10 cycles until only the low-level turbulence due to σ_v is still present. Figures 10b and 10c illustrate the increase in π required to achieve the cyclic behavior which we considered to be characteristic of a turbulent case. This criterion for transition was used to calculate the dashed curves for $\sigma_v = 0.035$ and 0.07 in Fig. 8.

To recapitulate the results of the two transition criteria, the alternating dashed lines in Fig. 8 qualitatively represent a "burst" or transient criterion for transition, while the dashed lines represent the particular (long-time) criterion. For the latter case, regions to the right of the nearly vertical line segments are indicated to be turbulent. The difference between the two criteria is in part explained by Eq. (4), which must be augmented by the term $\bar{\rho} <v> (\partial q^2/\partial y)$ when σ_v is finite. This can result in three different turbulence time scales being competitive in specific parametric cases.

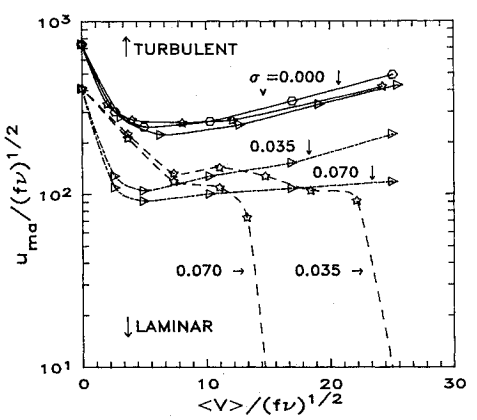

Fig. 8 Effects of injection and injection disturbance level on the stability of the acoustic boundary layer.

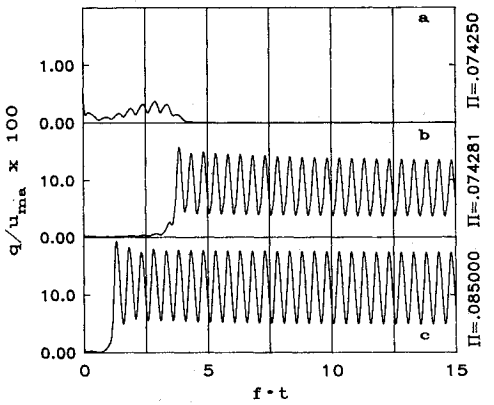

Fig. 9 Time variation of turbulence development for the injected acoustic boundary layer ($\sigma_v = 0$, $y = \delta_a$).

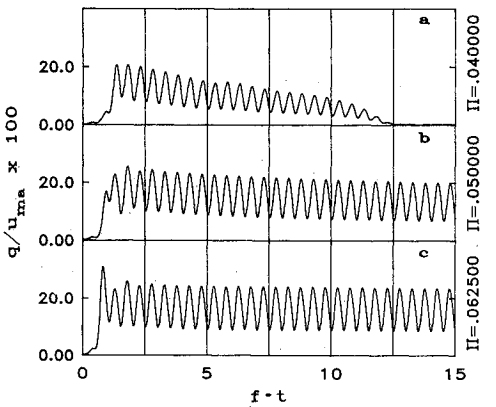

Fig. 10 Time variation of turbulence development for the injected acoustic boundary layer ($\sigma_v = 0.035$, $y = \delta_a$).

IV. Conclusions

An analysis of transitional and turbulent acoustic boundary layers in the presence of strong injection has been presented. The problem was approached by analyzing the behavior of a second-order turbulence model rather than by the traditional Orr-Summerfeld linearization. The approximate, order-of-magnitude analysis provides a simple and functionally correct estimate of transition for simple acoustic boundary layers. This technique may prove useful for estimating the stability characteristics of other types of flows.

The computed results for Stokes layers with injection indicate a substantial increase in the acoustic boundary-layer thickness for strongly injected laminar or turbulent flows, but no "blow-off" condition is observed. For injected, fully turbulent flows, a pronounced Richardson effect is obtained and is accompanied by very large maximum levels of turbulence (>20%). Both axial velocity and turbulence profiles exhibit a convected wave train shape. The turbulence development was also found to lag the rectified acoustic velocity by a few degrees at lower frequencies.

Transition results for conventional Stokes layers are in agreement with the approximate analysis and data trends, although at the higher acoustic amplitudes shown by the

scaling relation, additional nonlinear effects would be important. The effect of injection is to decrease (nonmonotonically) the critical acoustic Mach number for transition up to a factor of about three. This effect is frequency dependent but is expressible in terms of the acoustic and injection Reynolds numbers for the problem.

A further appreciable reduction in critical Mach number (or Reynolds number) is predicted for injection velocities with finite, continuous disturbance levels. This effect is strong enough to indicate that at the minimum critical acoustic Reynolds number, rather modest levels of acoustic pressure ratio ($\sim 1\%$) can induce significant turbulence levels near the surface.

The potential for turbularization of a near-surface reaction zone in ducted flows such as rocket chambers, therefore, theoretically exists. Whether this mechanism can produce instability in such systems, however, depends upon several effects not considered in this investigation. For example, combustion processes and (acoustically) nonlinear behavior such as thermoacoustic streaming could influence the nature of the overall response, whereas the axial mean flow could bias the transitional characteristics over the acoustic velocity and pressure cycles. Further research on these topics is in progress.

Acknowledgment

This research was supported, in part, by the Air Force Office of Scientific Research (AFSC) under Grant AFOSR 85-0348. Drs. Leonard Caveny and Robert Vondra were Program Managers.

References

[1]Culick, F. E. C., "Stability of Longitudinal Oscillations with Pressure and Velocity Coupling in a Solid Propellant Rocket," *Comb. Sci. and Technology*, Vol. 2, No. 4, Dec. 1970, pp. 179–201.

[2]Lengellé, G., "A Model Describing the Velocity Response of Composition Propellants," *AIAA Journal*, Vol. 13, March 1975, pp. 315–322.

[3]Brown, R. S., Willoughby, P.G., and Dunlap, R., "Coupling Between Velocity Oscillations and Solid Propellant Combustion," AIAA Paper 84-0288, January 1984.

[4]Brown, R. S., Blackner, A. M., Willoughby, P. G., and Dunlap, R., "Coupling Between Velocity Oscillations and Solid Propellant Combustion," *Journal of Propulsion and Power*, Vol. 2, Sept. 1986, pp. 428–437.

[5]Beddini, R. A., "Injection-Induced Flows in Porous Walled Ducts," *AIAA Journal*, Vol. 24, Nov. 1986, pp. 1766–1773.

[6]Flandro, G. A., "Non-linear Transient Combustion of a Solid Rocket Propellant," AIAA Paper 83-1269, June 1983.

[7]Glick, R. L. and Renie, J. P., "On the Oscillatory Flowfield in Solid Rocket Motors," *Proceeding of the 20th JANNAF Combustion Meeting*, Chemical Propulsion Information Agency, Vol. 1, Oct. 1983, pp. 143–160.

[8]Ben Reuven, M. "The Viscous Wall-Layer Effect in Injected Porous Pipe Flow," *AIAA Journal*, Vol. 24, Feb. 1986, pp. 284–292.

[9]Hedge, U. G., Chen, F. L., and Zinn, B. T., "Investigations of Reactive and Non-reactive Acoustic Boundary Layers on Porous Walled Ducts," AIAA Paper 85-0235, Jan. 1985.

[10]Baum, J. D. and Levine, J. N., "Numerical Study of Flow Turning Phenomenon," AIAA Paper 86-0533, Jan. 1986.

[11]Merkli, P. and Thomann, H., "Transition to Turbulence in Oscillating Pipe Flow," *Journal of Fluid Mechanics*, Vol. 68, Part 3, April 1975, pp. 567–575.

[12]Gostinsev, Yu. A. and Pokhil, P. F., "Relation of Two Combustion Anomalies of Powder Tubes," *Doklady Akademii Nauk SSSR, (Soviet Physics—Doklady)*, Vol. 188, No. 1, Sept. 1969, pp. 135–136.

[13]Keith, H. G. and Purdy, K. R., "Laminar Forced Convection under the Influence of a Resonant Acoustic Field," *Proceedings of the 1967 Heat Transfer and Fluid Mechanics Institute*, edited by Libby, Olfe, and Van Atta, Stanford Univ. Press, Stanford, CA, 1967, pp. 298–315.

[14]Lin, C. C., "Motion in the Boundary Layer with a Rapidly Oscillating External Flow," *Proceedings of the International Congress on Applied Mechanics*, Vol. 4, University of Brussels, Brussels, Belgium, 1957, pp. 155–167.

[15]Lin, C. C., *Theory of Hydrodynamic Stability*, Cambridge Univ. Press, Cambridge, England, 1955, Chap. 3.

[16]Donaldson, C. duP., "Calculations of Turbulent Shear Flows for Atmospheric and Vortex Motions," *AIAA Journal*, Vol. 10, Jan. 1972, pp. 4–12.

[17]Varma, A. K., Beddini, R. A., Sullivan, R. D., and Donaldson, C. duP., "Application of an Invariant Second-Order-Closure Model to the Calculation of Compressible Boundary Layers," AIAA Paper 74-592, June 1974.

[18]Schlichting, H., *Boundary Layer Theory*, 6th ed., trans. by J. Kestin, McGraw-Hill, New York, 1968, p. 421.

[19]Beddini, R. A., "A Preliminary Investigation of Fluid Dynamic Aspects of Combustion Instability in Solid Propellant Rocket Motors," U.S. Air Force Rocket Propulsion Lab., Edwards AFB, CA, TM82-01, Dec. 1981.